PIDECα: PHOTON INTERMEDIATE DIRECT ENERGY CONVERSION USING THE ALPHA EMITTER POLONIUM-210

A Dissertation presented to the

Faculty of the Graduate School at the

University of Missouri

In Partial Fulfillment of the

Requirements for the Degree

Doctor of Philosophy

---

by

CHARLES L. WEAVER III

Dr. Mark A. Prelas, Dissertation Supervisor

JULY 2012

The undersigned, appointed by the dean of the Graduate School, have examined the dissertation entitled

PIDECα: PHOTON INTERMEDIATE DIRECT ENERGY CONVERSION USING

THE ALPHA EMITTER POLONIUM-210

Presented by Charles L Weaver III,

A candidate for the degree of Doctor of Philosophy,

And hereby certify that, in their opinion, it is worthy of acceptance.

Dr. Mark A. Prelas

Dr. Tushar K. Ghosh

Dr. Sudarshan K. Loyalka

Dr. Robert V. Tompson

Dr. Dabir S. Viswanath

Mom and Dad

My wife[*]

Mum

fine, John too

[*] She forced me to put her name in here! Can you believe that? No respect…

ACKNOWLEDGEMENTS

This exists because of support from the following people:

- Dr. Prelas, who let me engage in work I found interesting and my committee, who humored me by sitting through the presentation
- The rest of the NSEI faculty, who put up with me during my time at Mizzou
- Students-turned-Doctors Robert Schott, Jay Rothenberger and Eric Lukosi. Respectively, they showed me the ropes of PIDEC and answered my inane questions, designed the first MCNPX model of the system, and measured the alpha spectrum of the Po-210 source. Generally, they were patient and let me know when ideas were bad, insufficient, or just plain wrong.
- Latricia Vaughn and James Bennett, the essential elements of every student's graduation fault tree.
- The Department of Education, who funded this
- The University of Missouri Graduate School who made things so interesting.

TABLE OF CONTENTS

TABLE OF FIGURES

TABLE OF TABLES

ABSTRACT

This work details the development of two proof-of-concept Photon Intermediate Direct Energy Conversion systems using the α-emitter Po-210 (PIDECα). Ch. I begins with a short history of nuclear battery development and then describes the expansion nuclear battery technology. It includes a review of recently published alphavoltaics in the literature, some shortcomings they exhibit, how these can be avoided with PIDEC, and the previous results seen with PIDEC systems. Ch. II describes the radioisotope sources used in the literature and compares their relative benefits.

The remaining chapters discuss the fabrication and testing of the gas- and solid-state PIDEC devices. Ch. III reviews the theory of PIDEC and describes the models used to predict the behavior of the systems. Ch. IV details the design and assembly of the experimental apparatus. Ch. V contains the methods used to enact the experiments. Ch. VI presents the results of the experiments and analysis of those results. Ch. VII contains the conclusions drawn from the work and methods for improvement beyond the proof-of-concept phase. Both systems demonstrate the conversion of kinetic energy into electrical energy by PIDEC. The results of the gas fluorescer system are encouraging; photon transport efficiency was hampered as may be useful after some improvements. The Gallium Phosphide (GaP) results currently discourage application in long-lived batteries.

1. HISTORY / MOTIVATION

1.1 Introduction

Certain places require electricity sources which are portable, durable, and long-lived. For example, space exploration in areas where starlight is insufficient to allow for the use of solar power aboard satellites, or places which are so cold that conventional chemical batteries cannot function. In these places, the high specific power and appropriately long half-life of radioisotopes can make them a good candidate for a power supply in a device called a nuclear battery. Nuclear batteries use the energy of radioisotope decay to produce electricity, rather than the chemical energy of traditional batteries. The idea of a nuclear battery was introduced in a 1913 betacell patent by G. H. Moseley. The subset of nuclear batteries which use α-emitters, called alphavoltaics, were designed in the late 1950s; they were introduced to the world in 1959 by then-President Dwight D. Eisenhower[1] Since 1961, radioisotope power supplies (RPSs) have been employed in numerous satellites missions [2]. Until very recently these RPSs have all been of a single design called the Radioisotope Thermal Generator (RTG). Despite the strong record of RTG performance, two of their characteristics leave room for improvement. First, the persistently high price of putting mass into orbit introduced the additional criterion of cost-effectiveness. Second, the limited radioisotope supply pressured designers to extend the effective life of the Plutonium-238 supply. These two criteria are both satisfied by a common goal: increased system efficiency. By increasing overall conversion efficiency, advanced nuclear batteries would produce the same amount of power while reducing weight and radioisotope mass. This interest in increased

efficiency has spurred on new multi-Watt nuclear battery research which recently culminated in the introduction of several new technologies[3]. These state-of-the-art multi-Watt nuclear battery designs claim energy conversion efficiencies over 27%[4] using the same 250 W_{th} General Purpose Heat Sources (GPHS) found in early RTGs, which reported initial efficiencies around 5%[1].

Concurrent with ongoing multi-Watt battery research, the field of Micro-ElectroMechanical systems (MEMS) has produced sensors which require reliable, long-term delivery of micro- and nano-watts which can be met through small nuclear batteries. Devices in the literature which hope to fill this demand use a variety of mechanisms to do so, and the results of these efforts indicate varying degrees of success. Regardless of scale, multi- and micro-Watt research groups alike seek products with similar characteristics: a power source which is robust, long-lived, efficient and cost-effective. If a design is also scalable, all the better. PIDEC alphavoltaics (PIDECα) are one method of theoretically achieving these five goals. To that end, this work investigates the behavior of two proof-of-concept PIDEC devices. One uses a rare gas fluorescer; the other, a solid-state semiconductor crystal. To highlight why PIDEC may be advantageous it is useful to first discuss how nuclear batteries are classified and to then present the common issues encountered by recent battery designs in the literature, available in Table .

Table 1: Recent Alphavoltaics

Year	Investigator	Isotope	Device Class	Method
1969	NARC	Pu-238	Indirect Conversion	Ar Gas Fluorescence
1996	Rybicki	Am-241	Indirect Conversion	SiC illumination
2004	Snyder	Cm-244	Indirect Conversion	Liquid Gallium
2005	ERI/Notre Dame	Pu-238	Indirect Conversion	Thermoelectric
2005	CSU[†]	Pu-238	Heat Cycle	SRG
2006	Cress et al.	Po-210	Indirect Conversion	InGaP illumination
2007	Hassan et al.	N/A	Direct Collection	Cantilever Theory
2008	Sychov et al.	Pu-238	Indirect Conversion	Phosphor
2008	Cress et al.	Po-210	Indirect Conversion	Rare-Earth Phosphor
2011	Qiao *et al.*	Am-241	Indirect Conversion	SiC illumination
2009-Present (This work)		Po-210	Indirect Conversion	PIDECα

1.2 Nuclear Battery Overview

A majority of small-scale nuclear batteries in the literature have been betavoltaics, but several properties of α -particles make them ideal for use in compact battery systems under appropriate supervision. Of all α-emitters, only a select few are appropriate for use in radioisotope battery production due to a combination of parameters. All nuclear batteries, regardless of the isotope they use, are classified under one of three distinct archetypes[5]: heat cycle, direct conversion, or interaction-energy. Each archetype is distinguished by the mechanism used to harness the decay energy. The overwhelming majority of alphavoltaics in service have been heat cycle devices, but several devices from each category have become available in the recent literature as seen in Table I.

RTGs are the most commonly deployed alphavoltaic; they are examples of the most common category of nuclear batteries: heat cycle devices. These batteries first convert the kinetic energy of emitted particles into heat within a system component. This

[†] Cleveland State University, University of Minnesota, Gedeon Associates, Sunpower and Stirling Technology Company (STC) were collaborators in this research.

heat is then used to produce electricity. RTGs accomplish this by the Seebeck effect, where a temperature gradient across two ends of a thermocouple induces a thermoelectric voltage *V*. The nuclear battery applies this differential voltage across two ends of a reactive load *Z* which results in a current *I* through the load. As mentioned previously, RTG batteries are an established technology; in some cases these original RTGs continue to provide power well beyond the expected lifetime of the satellite[2]. RTGs were recently replaced by Stirling Radioisotope Generators (SRGs) which use the Stirling heat cycle to heat Helium gas and drive a piston at the head of a linear alternator. Despite efficiency improvements, these are complex devices which have moving parts, increasing weight and cost.

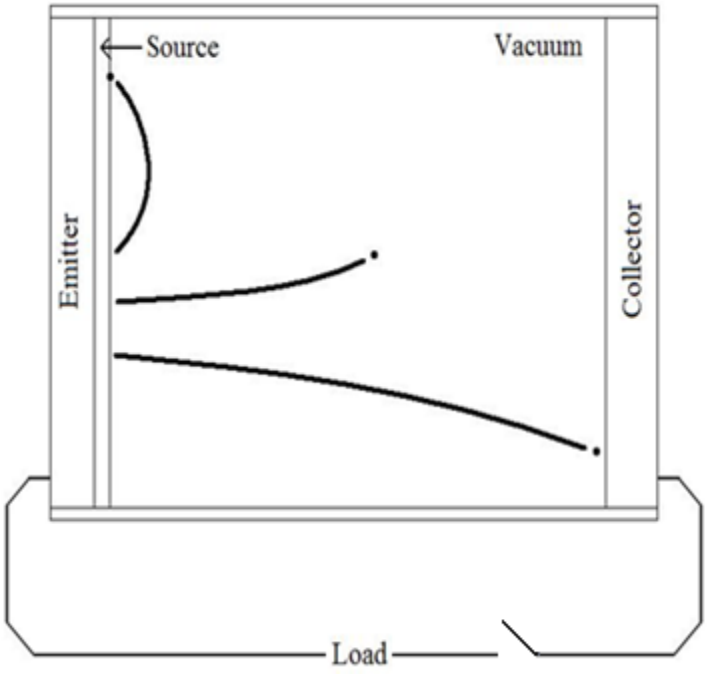

Figure 1: Diagram of Direct Collection Cell[5]

Batteries of the second archetype, direct collection, rely on the charge of an emitted particle to produce e lectricity rather than kinetic energy. A simple example of a

direct collection scheme is available in Fig. 1[‡]. As charged particles are emitted from a thin radioactive source located in the emitter electrode on one side of a cell; they pass through the cell's interior to the collector electrode, located opposite of the emitter, which accrues charge as particles continuously collide with it. Once a path is provided for charge to flow from the region in which it is collected back to the emitter electrode, the charge redistributes itself and current flows through the load. The only recent direct-collection device in the literature[6] is theoretical. It replaces the source in an existing betavoltaic cantilever[7, 8] with an α-emitter. As the isotope decays, ionizing particles collide with the cantilever arm. The energetic α-particles induce a net charge on the cantilever surface in two ways: by ejecting electrons off of the cantilever surface in high-energy collisions and stripping electrons from the copper cantilever as the positively-charged Helium nuclei lose energy. As a positive charge builds up on the cantilever surface it is attracted to a plate beneath the cantilever until the two become close enough to discharge, which allows the charge to redistribute in the form of flowing current. Further, the fixed end of the cantilever arm is attached to a piezoelectric plate so, once the free arm contacts the adjacent plate it oscillates and produces an AC voltage signal whose parameters depend on the design of the system. The benefits of this system over the betavoltaic embodiment are described as: better charge collection/lower leakage, higher specific power and thinner cantilever arms. In contrast, it also offers significant drawbacks which make α-particles inappropriate for this system. A shorter oscillatory period makes it a poor option for running machines which require high power and its efficiency is much lower than similar betavoltaics.

[‡] Particle deflection occurs in Fig. 1 as charge accrues on the collector plate, increasing the electrostatic force encountered by particles leaving the emitter plate.

Last is the family of interaction-energy conversion devices, which includes the work described in Ch. IV-VI. Interaction-energy devices are largely defined by what they are not: they rely neither on collecting the charge of emitted particles' nor on the production of heat in the system. What defines an interaction-energy device is that the incoming energetic particles interact with the system in some way, by excitation or ionization, which eventually results in the production of current. Several interaction-energy nuclear batteries in the literature used a semiconductor depletion layer [9-11] as the transducer, turning the specific ionization created by α-particle into electron-hole pairs. Within the depletion layer the intrinsic electric field forces the pairs are swept apart to produce charge. This class of devices is handicapped because of mismatched scale lengths[12] which occurs when α-particle range is greater than depletion region width but they exhibit a more severe deficiency. Systems which rely on interactions between α-particles and the depletion layer experience rapid degradation in short order. Incoming particles dislocate atoms which create the depletion region, and this dislocation has two important consequences.

First, dislocations interrupt the structure of the depletion region which decreases the overall strength of the electric field within it. As electric field strength decreases, electron-hole pairs produced during ionization are separated less forcefully. This diminishing force means charge carriers (AKA the current) move more slowly towards their respective ends of the p-n junction, which increases the chances for recombination before reaching the boundary. So, as more and more defects are introduced, current decreases because charge carriers are less and less directed where to go. The second major consequence of these dislocations is that they serve as traps. Traps capture charge

carriers, which further prohibits current flow.

To combat the decay found in direct illumination devices, results in the literature look for materials more resistant to radiation damage; others prevent the source from directly illuminating the depletion region by use of an intermediary. Investigators have shown that annealing after exposure repairs some function as dislocated atoms return to their proper lattice location [13]. If the device produces enough waste heat to self-anneal, this occurs during operation and the battery can continue to produce most of its initial power throughout its useful life; most but not all. Another method for mitigating radiation damage sandwiches an intrinsic semiconductor layer between the p- and n-doped regions of the radiation-resistant material InGaP. This delays device failure but not sufficiently[14].

The most success encountered in combating radiation damage occurs after introducing an intermediary to the system which absorbs radiation damage. In order for this strategy to be successful however, the intermediary itself must be either immune to radiation damage or resistant enough to survive throughout the useful life of the battery. Developments in solid-state intermediates have focused on improving radiation hardness. Two recent results in the literature have investigated the effect of phosphor doping to improve the radiation-hardness of phosphors [15, 16]. Since the phenomenon of radiation-induced phosphor degradation is well-known [17], the contribution of these experiments is in developing radiation-hard phosphors. Most results exhibit undesirable instability due to radiation damage; for some this rate of damage is small but none exhibit no degradation.

For liquid- and gas-phase materials, radiation damage is less of an issue because

the high specific ionization produced by α-particles does not disrupt the device in an irreversible way, in theory. For example, a recent liquid alphavoltaic patent[18] sandwiches Gallium metal between two metals, Iridium and Zirconium. As ionizations occur within the Gallium, the difference in work function between the two metals causes ions to migrate to the Zirconium and free electrons to the Iridium. It claims nearly 60% efficiency, using one Curie of Cm-244 to produce 20 mW of power at a 1.6 V potential but does not discuss the possibility of current loss due to electron-ion recombination or electrode corrosion. A patent [19] which uses the visible radiation produced by α-particle interactions with a rare-gas plenum avoids the issue of radiation damage. A sphere covered with photovoltaic cells covers the plenum, which houses the radioactive source at the center. It claims to produce 550 μW_e from 27 Ci of Pu-238 for a system efficiency of 2.4×10^{-3} %. A majority of these interaction energy devices are predated by PIDEC systems. Prelas *et al*[20, 21] recognized the need for an intermediate transducer to produce power without degrading performance; PIDEC was the result. Previous attempts have been modeled and demonstrated using a variety of ionizing particles and fluorescers [20-23], but not α-particles. The two proof-of-concept PIDEC alphavoltaics developed for this work used solid-state Po-210 sources in conjunction with gas and solid fluorescers. PIDEC systems generally allow for a high theoretical efficiency which is determined by fluorescer and transport efficiency.

2. ISOTOPE CHOICES

Table 2: Radioisotopes in the Literature[24]

Isotope	$T_{1/2}$	Decay Radiation (eV)	Daughter (Decay, $T_{1/2}$)	Comments
Po-210	138.4 d	α: 5.30 (100%)	Pb-206 (stable)	
Pu-238	87.7 y	α: 5.50M (70.9%) 5.46M (21%) γ: 13.6k (10.2%)	U-234 (α/SF, 2.46 Ga)	Fertile SF (1.9E-7 %)
Am-241	432.6 y	α: 5.49M (84%) 5.44M (13.1%) γ: 13.9k (37%) 59.5k (36%)	Np-237 (α/SF, 2.14 Ga)	Fertile SF (4E-10 %)
Cm-244	18.1 y	α: 5.80M (76.9%) 5.76M (23.1%) γ: 14.3k (9%)	Pu-240 (α/SF, 6.56 ka)	Fertile SF (1.4E-4 %)

The α-emitters used in the literature are Po-210, Pu-238, Am-241, and Cm-244; a comparison of their characteristics is available in Table 2. Several results available in the literature used Am-241. Multi-Watt batteries currently use Pu-238 manufactured by the Space and Security Power Systems Facility (SSPSF) at INL. The sources used in these experiments were Po-210 sealed sources with initial activity A_0 of 0.8 and 5 mCi. All α-emitters require appropriate precautions for safe handling due to the radiological and toxic hazards they present[25]. When safely employed, the properties of each source make them apropos to certain parts of the development cycle. Po-210 is most appropriate for short-term research work due to a 138-day half-life, which results in shorter oversight periods. Po-210 has a monoenergetic emission with no significant high-energy photon or electron emissions. Its stable Pb-206 daughter product presents no additional radiation hazard. Commercially-available sources are also cost-competitive if one knows where to

look. Pu-238 has been the isotope of choice in RTGs for the past forty years. It provides good alpha emission with relatively low photon and neutron emission. It has a small chance for spontaneous fission. Am-241 is another suitable isotope which exhibits close alpha emission energies and lower fission occurrence than Pu-238. Its high incidence of photon emission, although low-energy, may require shielding of the adjacent environment.

3. PIDEC THEORY AND MODELING

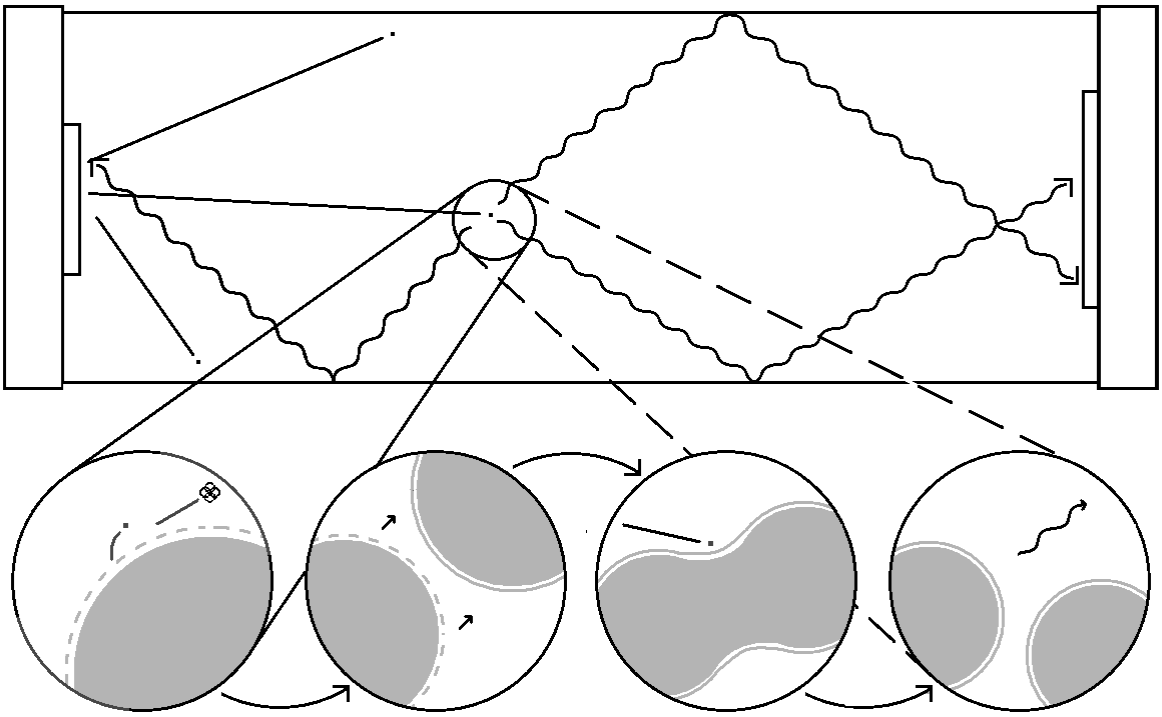

Figure 2: PIDEC process reactions (not to scale) featuring (left to right, top to bottom): (top) alpha particle emission, excimer gas interactions, and photon collection at the photodiode; (bottom) ionization of the electron cloud (grey), excimer formation, electron collision, excimer decay, and photon emission.

Like several other interaction energy devices, PIDEC alphavoltaics produce current using a radioactive source, an intermediate transducer and a collector which produces current. The transducers used in these two experiments are fluorescers, and the collector is a photovoltaic cell. One uses the rare gasses Xenon and Argon, the other uses a solid-state Gallium Phosphide (GaP) semiconductor crystal. Once α-particles leave the

source they encounter the fluorescer. Figure 2 shows this process for a gas-fluorescer, with α-particles leaving the source and entering a gas plenum. As α-particles interact with the fluorescer, they ionize and excite whatever components they collide with. When α-particles interact with the constituent atoms of the gas plenum, ions, free electrons, and excited atoms[§] are formed. This average fraction of initial α-particle energy which is deposited in the gas is the energy deposition efficiency η_d. The fluorescer efficiency, η_f, is determined by the fraction of interactions which produce light, either by an excimer or interaction. With no external voltages being applied in these experiments, the expectation may be that the electrons, ions, and excited atoms created during α-particle interactions will recombine and emit line radiation. This is essentially the process for semiconductors; the process is more complex for gases. Because this fluorescer light is emitted isotropically, it must be directed toward a photovoltaic cell using a waveguide. The fraction of photons, and therefore energy emitted by the gas, which reaches the photovoltaic is termed the transport efficiency, η_{tr}. Upon reaching the photocell, the photon is absorbed in the depletion region and an electron is simultaneously injected into the conduction band. The newly created electron-hole pair is then swept out as current.

The total efficiency η_{tot} of this energy conversion process, from atomic decay to photovoltaic current, can be expressed in two equivalent ways as seen in Eq. 1; the four efficiency terms within it are determined by the design of the system. It can be seen as either the product of the efficiencies along each step[21] or as the power produced by the photovoltaic divided by the power emitted by the source. A condensed explanation of the

[§]Free electrons typically have sufficient energy to produce additional ionization and excitation with other atoms in the gas.

variables found in Eqs. 1-3 is available in Table II.

$$\eta_{tot} = \eta_d \cdot \eta_f \cdot \eta_{tr} \cdot \eta_{PV} = P_{PV}/P_{src} \quad (1)$$

$$P_{PV} = I_{PV} \,/\, R \quad (2)$$

$$P_{src} = E_\alpha \cdot A_0 \cdot e^{-\lambda t} \quad (3)$$

$$\eta_{PV} = \eta_{DP} \cdot FF \cdot E_g/E_\gamma \quad (4)$$

Table 3: Explanation of Variables

Variable	Description
η_{tot}:	Total process efficiency
η_d:	Average fraction of α-particle energy deposited in gas plenum
η_f:	Excimer formation efficiency
η_{tr}:	Photon transport efficiency
η_{PV}:	Photovoltaic efficiency for photons of specified wavelength
P_{PV}:	Power produced by photodiode (W)
P_{src}:	Power emitted by source (W)
I_{PV}:	Current measured by picoammeter (A)
R:	Photovoltaic responsivity (A/W)
E_α:	Alpha particle energy at emission (5.3 MeV)
A_0:	Initial source activity (27.2 MBq)
t:	Time of experiment after receipt of source (days)
λ:	Decay constant of source (0.005023 day^{-1})
η_{DP}	Photovoltaic driving potential efficiency
FF	Photovoltaic fill factor
E_g	Energy band gap of photovoltaic
E_γ	Energy of excimer photon

Photovoltaic power is calculated in Eq. 2 using the emitted current I_{PV} and responsivity R at the peak excimer wavelength. The power emitted by the source P_{src} is calculated in Eq. 3 using the expected energy of the α-particle E_α, the initial activity of

the source A_0, decay constant of Po-210 λ, and time t between source receipt and experiment. Photovoltaic conversion efficiency was calculated using the common method in Eq. 4 and the peak excimer wavelength in Table 5: Maximum Excimer Fluorescence and Photovoltaic Efficiencies.

3.1 Rare Gas Fluorescer

Rare gas fluorescers rarely produce resonance or line radiation under the conditions used in these experiments. Instead, the dominant reactions occurring in rare gases with pressure between 0.5-3 atm (380-2280 Torr) [26, 27] lead to excimers formation. As alpha particles, or secondary electrons, careen through the rare gas it ionizes some of the atoms composing it. As shown in the literature, the numerous ionized atoms, excited atoms, and electrons quickly interact in three-body processes[28] which proceed to interactions between gas atoms with excited valence electrons and adjacent neutral atoms which form a bound excimer with molecular potential energy occupying one of the upper bound states as seen in the simplified Ar_2* energy level diagram of Fig. 5.

[Removed for Copyright]

Figure 3: Simplified Diagram for Ar_2 Excimer System (Source: Kiik et al[29])*

The excited electron in these bound *exci*ted di*mers* quickly[**] returns to the ground state and emits a characteristic 2nd continuum VUV photon in the process. The electron shells now filled, the negative charges of the electron clouds repel the unbound rare gas atoms. The process then begins again as incoming particles induce more excitation. The wavelength of the photon it emits is particularly dependent where the molecule is in the potential when it returns to the ground state. The central wavelength of the narrow excimer band depends on the gas species as well as the state of the excimer. For Ar_2* or Xe_2* at room temperature between a pressure of 0.5-3 atm[26], these central wavelengths are 126 and 172 nm respectively[21, 29].

The conversion, fluorescer, and photovoltaic efficiencies for the gas fluorescer system were estimated to high confidence through modeling, previous work, and calibration measurements. The unknown photon transport efficiency, η_{tr}, will be calculated using experimental results and Eqs. 1-4. Thin metal layers above the source foil which allow safe handling also decrease the average α-particle energy available for

[**] Excimer lifetimes are typically on the scale of ns.

ionization in the gas plenum; their net effect is that a particle with 5.30 MeV at creation is expected to have 5.0 MeV upon entering the gas plenum, lowering the maximum η_d from unity to 0.943. This expected α-particle energy was calculated from the α-particle energy spectrum using a Canberra 7404 alpha spectrometer. This spectrum was then converted into a histogram between energies of 4.4 and 5.4 MeV with 50 keV energy bin widths; it is available in Fig. 4.

Calculation of energy deposition efficiency began with energy spectrometry of the Po-210 α-source. To reduce modeling time, the energy spectrum of the Po-210 source was histogrammed into an energy distribution with 50 keV energy bin width. This energy distribution was then used in a MCNPX[30] model of the system to determine the fraction of energy deposited in the gas plenum for pressures between 53 and 267 kPa (400 - 2000 Torr). The results of the energy MCNPX energy deposition tallies in certain system components are shown in Table 4. Gas deposition efficiency η_d is calculated by multiplying the values in Table 4 by 0.943 to account for energy lost to the foil. The average α-particle energy deposition fraction η_d is determined by α-particle range and gas plenum scale length[21]. The system parameters which control α-particle range are initial particle energy, excimer gas pressure, and gas plenum species. Gas plenum scale length is determined by gas plenum pressure and system geometry. If the particle range is not well-matched to the scale length, i.e. if the particle range in the excimer gas is greater than the source-waveguide distance, η_d will be less than its theoretical maximum and particles deposit energy in the waveguide.

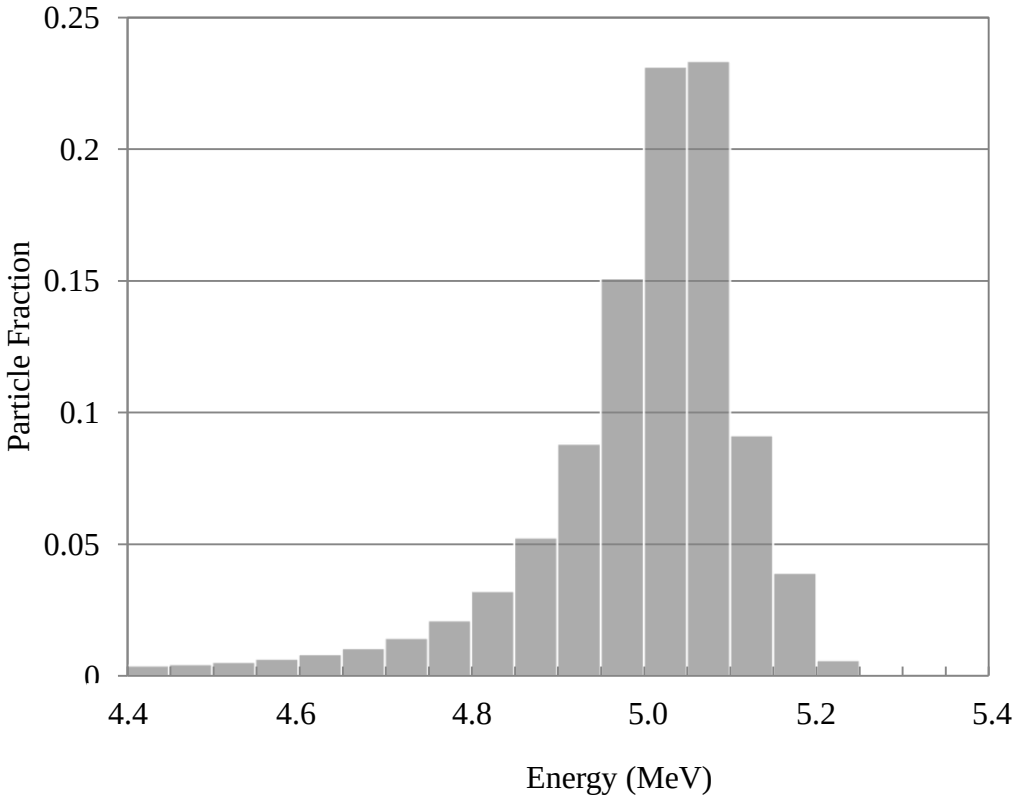

Figure 4: Alpha Particle Energy Distribution: 4.4-5.4 MeV

If the particle is not emitted toward the gas plenum, it is emitted toward either the base or lip of the source capsule. These two components have more influence on η_d than the foil because they absorb all energy of an incident α-particle. This is highlighted in Table 4 which shows that the largest fraction of average energy loss occurs in the base and lip of the source capsule, independent of excimer gas pressure. Also apparent in Table 4 is the necessity of proper scale length matching. At low plenum pressure a significant fraction of energy ends up in the waveguide. This undesired energy deposition has implications for the photon transport efficiency term η_{tr} which are discussed below. Increasing gas plenum pressure abates the undesired energy loss as more interactions occur within a denser gas plenum until energy deposition in the waveguide mirrors

becomes negligible. Thus higher gas pressure has two benefits for this specific geometry: increasing η_d, which results in more photon production by the gas, and preserving η_{tr}.

Table 4: Average Fraction of Energy Deposited in System Components

		Component							
Pressure		Plenum (%)		Mirrors (%)		Base (%)		Lip (%)	
(kPa)	(Torr)	Ar	Xe	Ar	Xe	Ar	Xe	Ar	Xe
53	400	8.52	16.6	35.8	29.0	49.2	49.6	4.9	4.3
80	600	13.3	24.9	31.8	21.3	49.3	49.7	4.7	4.0
107	800	18.4	32.2	27.6	14.2	49.3	49.9	4.6	3.7
133	1000	23.0	38.6	23.2	8.01	49.4	50.0	4.4	3.4
160	1200	27.2	43.5	19.0	3.23	49.5	50.1	4.3	3.1
187	1400	31.4	46.1	14.9	0.76	49.5	50.2	4.1	2.9
213	1600	35.3	47.0	11.2	0.06	49.5	50.3	4.0	2.7
240	1800	38.9	47.2	7.7	6×10^{-5}	49.5	50.4	3.9	2.4
267	2000	42.0	47.3	4.7	0.0	49.5	50.4	3.7	2.2

Excimer gas fluorescence efficiencies η_f , i.e. the fraction of ionizations which result in excimer formation, and the peak wavelength of emission for the Argon and Xenon gases used in these experiments are available in the literature[20, 27]; they are reproduced in Table 5 for ease of reference. As excimers do not absorb the light they emit, photons travel through the gas plenum without interaction until they are absorbed by the photovoltaic or a system component.

Table 5: Maximum Excimer Fluorescence and Photovoltaic Efficiencies

Excimer	λ (nm)	E_γ *(eV)*	η_f (%)	η_{PV} (%)
Ar_2^*	129	9.62	50	5.7
Xe_2^*	172	7.2	48	7.6

The photon transport efficiency η_{tr} is governed by two processes: line-of-sight travel and reflection. The transport efficiency of line-of-sight photons can be considered to be the total solid angle of isotropic light emission which falls within the field of view of the photovoltaic cell for any point within the ionization cloud. The contribution of this type of transport to η_{tr} is small. The reason for this is due to the isotropic emission of the source. Light produced near the photovoltaic has a larger solid angle which overlaps the field of view of the photovoltaic than light which is produced further away, but the amount of light produced in this way is small compared to the total amount of light produced by the gas. Most ionization in the gas plenum occurs immediately above the source. The reason for this is that all particles which deposit energy in the gas must deposit some energy directly above the source in order to travel further, but not all particles travel in the same direction. Consequently, most current from the photovoltaic is the result of photons which are transported by reflection. Light transport by reflection in this series of experiments is expected to be low because, returning to Table 4, the pressures used in experiment 1 result in some energy deposition in the mirrors. This energy deposition damages them, lowering their reflectivity and therefore photon transport of the system. In actual systems, waveguide damage is easily avoidable by using an appropriately high gas plenum pressure. The final step of PIDEC is photovoltaic conversion efficiency η_{PV}, determined by the energy of the incoming photon and the band gap of the photovoltaic as seen in Eq. 4[22].

Table 6: Po-210 Activities throughout Gas Experiments

Experiment	Gas Species	Activity (MBq)	Activity (μCi)
1	Ar	19.61	525
		19.24	520
		18.13	490
	Xe	17.39	473
		16.29	436
2	Ar	9.74	265
	Xe	3.35	90.5
3	Ar	7.81	211
	Xe	7.81	211

The activities of the Po-210 source used in the gas fluorescer experiments, initially 0.8 mCi, are available in

Table 6. To calculate the absolute and transport efficiencies, the recorded current I_{PV} and photovoltaic responsivity R are used in Eq. 2 to determine the power produced by the photodiode. The responsivity was previously calibrated by NIST in the visible and near-UV spectral regions (200-500 nm). The responsivity in the 100-200 nm wavelength was determined through comparison using a second photovoltaic which had been calibrated between 100-250nm. To accomplish this comparison, both photovoltaics were placed in a machined tray such that their centers were equidistant from the center of a tray. The center of the tray was then placed 60 cm above the center of a 3-color LED array. One LED was then turned on and the currents emitted by both photodiodes were

recorded simultaneously. The tray was then rotated ninety degrees and the measurements repeated; this process was repeated twice. These four measurement points were taken for each of the three LEDs as well as a dark current. The values were then averaged and the results are available in Figure 5. It was concluded that both photovoltaics exhibit similar responsivities in the 100-200 nm wavelength range based on: their similar responses under LED testing, their similar construction and their equivalent composition.

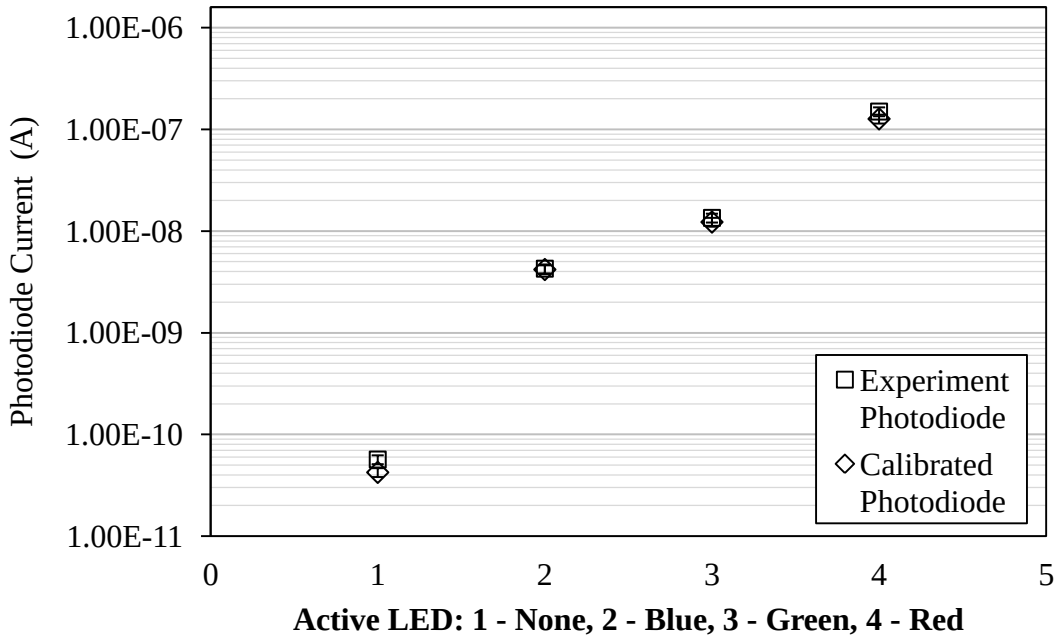

Figure 5: Photodiode Comparison

3.2 Gallium Phosphide (GaP) Fluorescer

When α-particles interact with semiconductors, they produce ionization. In semiconductors this ionization takes the form of electrons being ejected out of the valence band into the conduction band during ionization. When electrons settle back into the conduction band of a semiconductor, they may transition in one of two ways: radiatively or nonradiatively. During a radiative transition, the electron lose some energy

to produce light. In a direct band gap semiconductor crystal, these radiative transitions readily occur. In indirect band-gap semiconductors, such as GaP, the crystal must have the necessary momentum in order for radiative transitions to occur. If a radiative transition occurs, a characteristic photon will be emitted; for GaP this characteristic photon has a wavelength of 550 nm. If a nonradiative transition, occurs the energy is dispersed to the vibrational or rotational modes of the crystal. If defects exist the similar process of nonradiative quenching occurs where electrons in the conduction band are trapped, give up their energy to the lattice. The band structure of Gallium Phosphide (GaP) has three distinct emissions as shown in Figure 6: one direct and two indirect; the characteristic 550 nm radiative transition is phonon-assisted.

[Removed for Copyright]

Figure 6: Band Structure of GaP[31]

Modeling the efficiency terms of the GaP is in progress; thus these experiments investigate qualitative behaviors: whether the GaP emits light during α-particle interactions, and the effect of defect introduction rate on the light emitting characteristics of the crystal. As described in Ch. I, the effect of radiation damage on doped semiconductors is well identified; the effects of radiation damage on semiconductor light production is less examined. Estimates of defect introduction rates within the crystal were smaller than the atomic density of the crystal by many orders of magnitude. Consequently

it was theorized that some detector current decrease would be expected, but the rate of decrease would be small compared to the amount of light produced by the device.

4 APPARATUS AND ASSEMBLY

4.1 Rare Gas Fluorescer

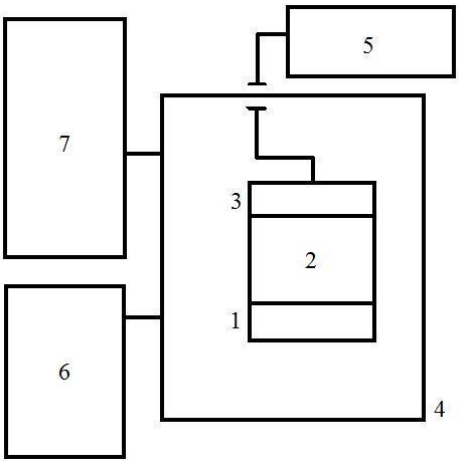

#	Component
1	Source
2	Plenum & Waveguide
3	Photovoltaic
4	Pressure Vessel
5	Picoammeter
6	Excimer Gas Tank (GCS)
7	Roughing Pump (GCS)

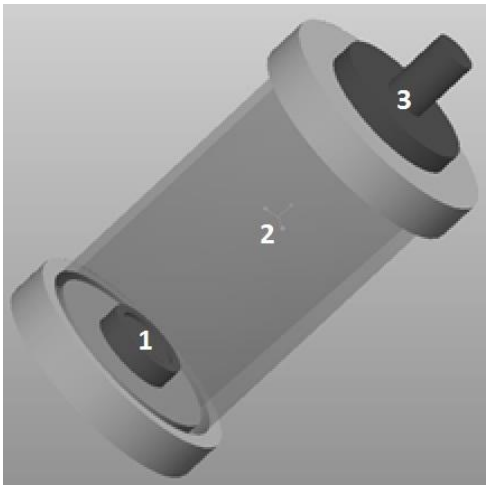

Figures 7 and 8: Block Diagram Drawing of System Components (Left), CAD drawing of Mirror Chamber (Right), and Legend (Center)

The experimental setup for the rare gas fluorescer system in Figures 7 and 8 required a: radioactive source, waveguide, Gas Control System (GCS)[††], pressure vessel, photovoltaic, UV filter, and picoammeter. To assemble the waveguide chamber, the source and photodiode were mounted in polished aluminum caps at opposite ends of the waveguide. This assembly was then placed within the pressure vessel. One set of fittings on a pressure vessel flange connected to GCS components while the photovoltaic inside the pressure vessel connected to the exterior picoammeter via a coaxial feedthrough located on a second flange. Three cylindrical waveguide mirrors of height 2.5, 5.1 and 7.6 cm and 3.1 cm inner diameter were fabricated using a thermal resistive evaporator. One set of four quartz glass substrates were cleaned with a mild detergent then rinsed with

[††] The Gas Control System consists of the Excimer Gas Tank, Roughing Pump, associated piping, and requisite valves

acetone, methanol, and deionized water. After drying, they were affixed within the evaporator and the evaporator chamber door was closed. Once a sufficient vacuum was reached, two thin films were deposited. The first film was 275 nm of Aluminum (Al) to ensure good reflection of light 100-200 nm in wavelength. The second was a 28 nm oxidation barrier of Magnesium Fluoride (MgF_2) to protect the Al films beneath. The excimer gases used in the experiments were research-grade ultra pure Xenon and Argon. Gas plenum pressure between 667 Pa- 667 kPa (5-5000 Torr) was measured using a MKS 722 Absolute Capacitance Manometer. The OSI optoelectronics UV100 inversion layer photodiode was connected to a Keithley 6487 picoammeter. Current data were recorded using the included Excelinx™ software.

The source used in this series of experiments was purchased from Eckert & Zeigler. It consisted of a rolled foil with initial activity 0.8 mCi and 5 mm active diameter. The foil was sealed in an A-2 capsule[32]. A suitable UV filter was found in a piece of soda lime glass, which exhibits a transmissivity cutoff for wavelengths shorter than 275 nm. The filter was prepared by cleaning a piece of soda lime glass with an Acetone-Methanol-Deionized Water (AMD) rinse; it was then left to dry.

4.2 Gallium Phosphide (Gap) Fluorescer

The GaP experimental setups in Figure 9 and Figure 10 required a: radioisotope source, source holder, fluorescer crystal, photon detector, current meter, circular rubber gasket, spacer plate, scissor jack, 550 nm line filter, spectrophotometer, and two light-blocking enclosures (light boxes). The items used depended on which of two sources was used. One apparatus used a low-activity source; this was the same 0.8 mCi source used in the gas fluorescer experiments. The second was a higher-activity source. This 5 mCi

source was sold by Amstat as a P2042 Nuclespot static eliminator. The semiconductor crystal was an intrinsic GaP crystal which had been covered with a layer of Aluminum on one side. Two photon detectors were used in these experiments: an OSI UV100 inversion layer photodiode, and an Oriel 77341 Side-On Photomultiplier Tube (PMT). These detectors used the Keithley 6487 and Oriel control box picoammeters, respectively. The PMT required a High Voltage Power Supply (HVPS).

Both systems required a common procedure to minimize intrusion of light created outside the experimental assembly into the system. First, all light routes for light created by sources outside the room were blocked off: door gaps, windows, holes in the wall which allowed in light from adjacent rooms. Second, all unnecessary light sources within the room were covered or turned off as appropriate, leaving enough light from the overhead fluorescent to assemble the necessary apparatus within it. All small gaps in the light boxes were taped shut with electrical tape. Once assembly of the low-activity or high-activity apparatus was complete, the overhead room lights were turned off and the experiment could proceed.

Assembling the low-activity GaP apparatus began with removing the detachable panels on the interior light box were. The interior box was then placed within the exterior light box. Next, the wiring for the appropriate detector was run to the center of the interior light box. The PMT was then immobilized on one of the detachable panels, with enough clearance to allow the GaP subassembly to be concentric with the PMT aperture, using a styrene block and zip ties. The PMT was then attached to the display and HVPS. Taking care to ensure that the wires fit smoothly through the holes on the detachable panel, the detachable side was then screwed into place and the gaps around the wiring

were taped shut with electrical tape. The scissor jack was then placed in the interior light box through the other detached panel. The GaP subassembly was then assembled on the scissor jack to be concentric with the PMT aperture. The spacer place was placed on the source holder so the active foil sat slightly above the hole in the center of the spacer plate. The rubber gasket was then placed on the spacer plate concentric with the source surface to form a 2 mm air gap before placing the GaP crystal near the source surface; this air gap is essential when using the low-activity source. The purpose of this air gap is to ensure that the delicate thin films which encapsulate the source foil do not make contact with the GaP surface. Doing so would easily scratch, dent, or rupture the source surface if something made contact with it. Once the GaP crystal was placed on the gasket, the lights were turned off within the room, the PMT HVPS and control box were turned on, the PMT was uncovered, and the scissor jack was raised until the GaP surface was flush with the PMT aperture. The remaining open panel of the interior light box was then taped closed, the exterior light box was closed and covered to cut down on light, and the system was ready for measurement.

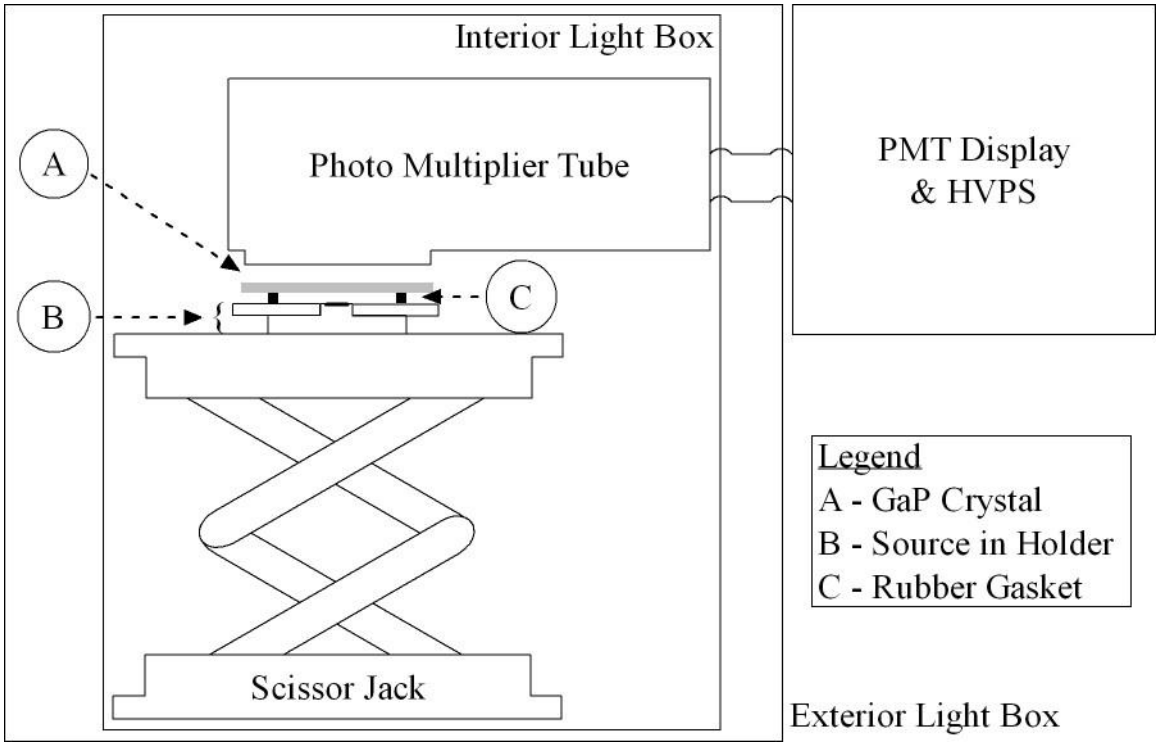

Figure 9: Low-Activity GaP Apparatus

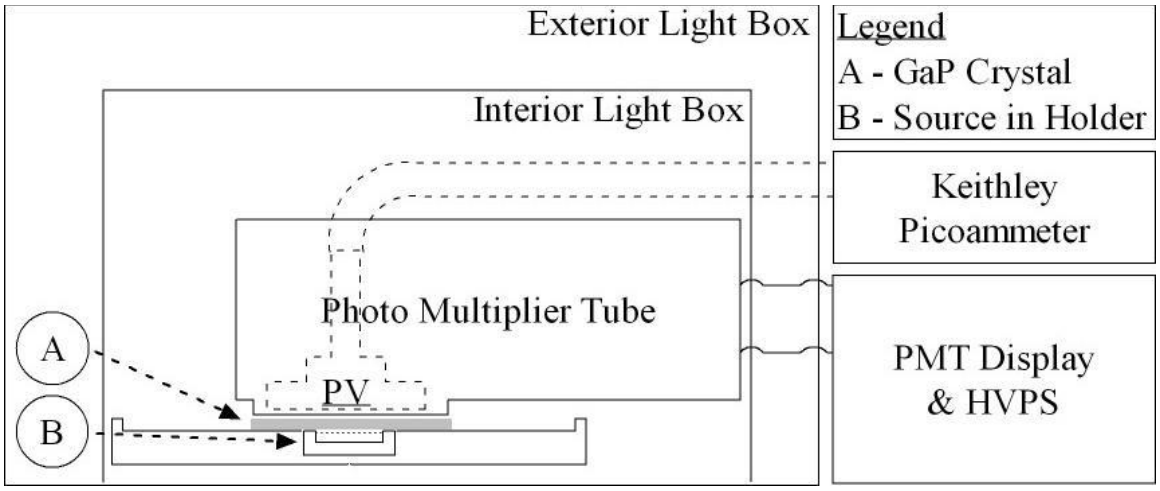

Figure 10: High-Activity GaP Setup

Observation of the photon generating stability of the GaP in the second series of experiments required the high-activity source. The requisite wiring was run into the

inside of the exterior light box and the appropriate measures were taken to minimize light from entering the box. The 5 mCi Po-210 source was then restrained in its holder using a screw and washer inside the exterior light box. The GaP crystal was then placed directly over the source; a gasket was not required due to the wire mesh and air gap which were built into the source holder to prevent contact with the source foil. Next, the detector was connected to the requisite control and measurement devices and placed over the GaP semiconductor such that it was concentric with the source. Once the detector was in place, the interior light box was carefully placed over the source holder and detector without disturbing it. The exterior light box was then shut, the control and measurement devices turned on, the lights were turned off and the system was ready for experiment.

5 EXPERIMENTAL METHOD

Multiple runs of five experiments were enacted in order to characterize the behavior of these alphavoltaics. Three were enacted to observe the certain characteristics of the gas fluorescer system: relationship between gas plenum pressure and PV current production, PV current over time at a constant pressure, and fraction of UV photon light production. The other two were performed using GaP semiconductor crystal. These were enacted to determine if photon production during α-particle illumination of the semiconductor crystal took place and characterize those photons, and observe photon generation over time.

5.1 Rare Gas Fluorescer

Before beginning any experiment, all connections were made and the system was assembled. The dark current was then measured to ensure proper connections between components were made during assembly. Next, a series of gas purges were enacted. This is essential because VUV-absorbing compounds in air adsorb onto the apparatus interior during maintenance and safety inspections. A pressure purge began by pressurizing the apparatus with Argon until reaching an interior pressure of 200 kPa (1500 Torr). Once the gas equilibrated, it was then evacuated using the roughing pump and refilled with Argon; this process was repeated five times.

The first experiment monitored changes in photodiode current with changing gas plenum pressure. The picoammeter was set up to average ten current values in order to minimize noise. This process was repeated one thousand times and the set of one thousand averages was then averaged to produce a point at each pressure value in the

figures below. Once the composite data point was calculated, the pressure was increased incrementally and the measurement process was repeated up to a maximum pressure of 200 kPa (1500 Torr). The pressure vessel was then slowly evacuated using the gas flow control system with data taken in the same pressure increments. Between current-pressure tests the pressure vessel was filled with Argon at ambient pressure to ensure that α-particles could not interact with the photodiode window.

The second experiment observes the longer-term behavior of the system using a method similar to the first experiment. The difference between these systems was waveguide. The waveguide used during experiment one was reused in experiment 2 when the pressure vessel was filled with Argon. This waveguide was replaced with a waveguide of height 76 mm before enacting experiment 2 using Xenon. The system was then tested and pressurized with an excimer species as normal. The photovoltaic current over a period was recorded using the picoammeter software. Duration of observation was controlled by sample delay trigger.

The third gas fluorescer experiment determined the relative spectral fractions of light emitted by the gas. The system was prepared as in the other second rare gas experiment with the addition of piece of soda lime glass placed in front of the photovoltaic. The system was then held at constant pressure and observed. Upon completion the slide was removed. The system was then reassembled and repressurized as normal and current data were recorded at the same pressure.

5.2 Gallium Phosphide (GaP) Fluorescer

Two experiments were enacted to measure the light emitted by a GaP crystal with time. The purpose of the first was to determine whether or not the presence of a Po-210 source would change the amount of current generated by a photomultiplier tube. This used both GaP experimental setups. For the low-activity source, the system was assembled first without the source present in the interior light box and PMT current was measured. Trial 0 determined an appropriate voltage to use throughout the rest of the experiments. A 750 V bias provided a reasonable signal with acceptable signal-to-noise ratio. The rest of the trials used the following procedure.

Before measurement the precautions described in the previous chapter were taken to ensure that exterior light was minimized. In position 0, the source was removed from the interior light box and the current was measured. In position 1, a piece of paper was inserted between the rubber gasket and GaP to prevent α-particles from reaching the crystal and the current was measured. In position 2, this piece of paper was removed to allow α-particles to interact with the GaP and the current was measured. Once it was established that there was an increase in current when the GaP was illuminated by α-particles, the apparatus was assembled in position 3. A 550 nm line filter was placed in the PMT aperture and the current was measured. The PMT was then replaced with the spectrophotometer used for photovoltaic comparison and the photon spectrum within the interior light box was measured using the longest integration time available: one minute. This procedure was repeated with the high-activity apparatus using both detectors.

Current stability monitoring used the high-activity source with both detectors, one at a time. The Keithley Excelinx software averaged 20 points with a slow integration time

to minimize noise and record photovoltaic current over 3 hours. To determine if the results were a consequence of equipment failure, the photovoltaic was replaced with the PMT and the PMT current was recorded periodically for comparison.

6 RESULTS AND ANALYSIS

6.1 Uncertainty

Random uncertainty for measurements made using the PMT was determined to be the difference between the average current observed in the PMT display over a 10 second interval and the greatest departure from that average. Relative systematic uncertainty for the PMT system was estimated to be 1%. The random uncertainty for results which used the Keithley was determined to be the standard error of the results of the run in position 2; this was done to prevent problems encountered when measuring very small currents which fluctuate between positive and negative values. Relative systematic uncertainty Current measurements which used the Keithley the systematic uncertainty was again estimated to be 1%. Relative uncertainty in η_d from MCNP models was less than 1% due to the number of particles used; this was combined with the relative uncertainty of the measured current. Relative uncertainty of fluorescer efficiency was not reported and assumed to be 2%, the difference between maximum theoretical fluorescer efficiency and the consistently measured experimental results available in the literature. Total relative uncertainties for the photovoltaic responsivity, photovoltaic conversion efficiency, and pressure sensor readout were 2% or less according to NIST –traceable calibrations. All uncertainties were added in quadrature as appropriate to calculate the total relative uncertainty in photon transport efficiency.

6.2 Rare Gas Fluorescer

The results, peak performance characteristics, and corresponding efficiencies of experiment 1 are available in Figure 11, Table 7, and Table 8 respectively. The results

exhibit several notable behaviors: hysteresis within a trial, similar current-pressure curves among trials, and a net decrease in current between trials.

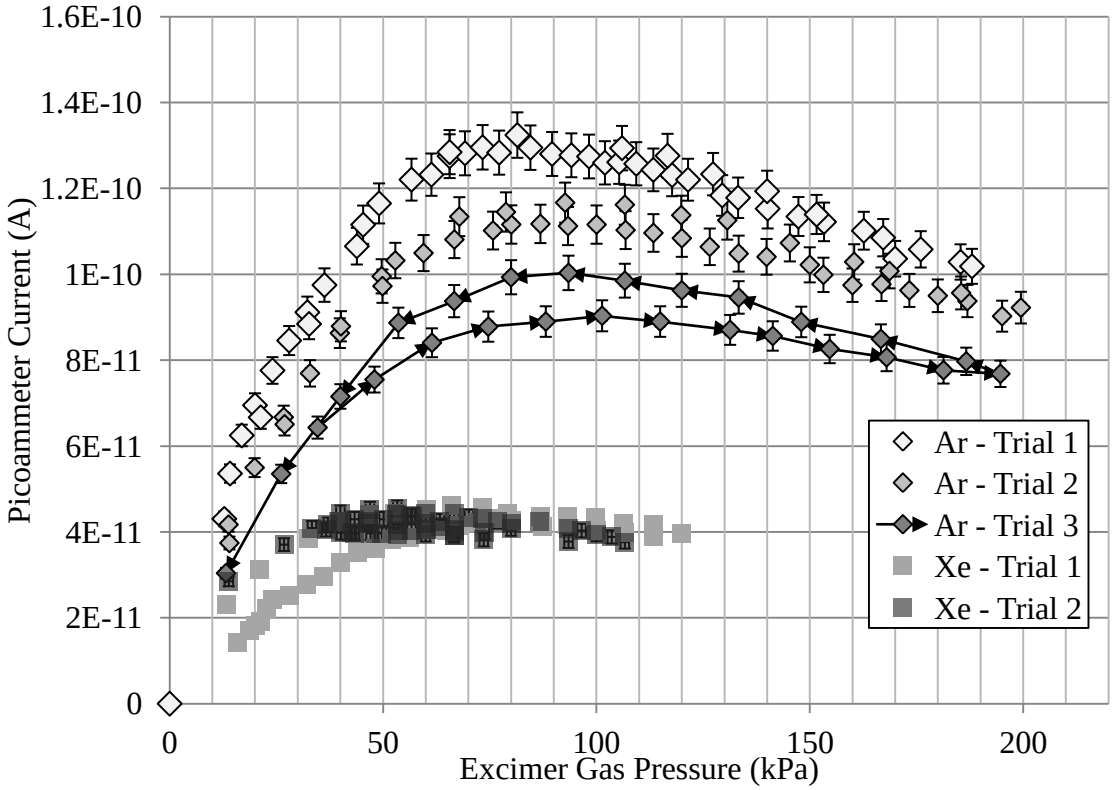

Figure 11: Experiment 1 Results

The appearance of hysteresis in the results is not surprising; it is commonly encountered in diaphragm pressure sensors. As pressure within a run increases or decreases the diaphragm can slightly deform and introduce a small systematic error. However, hysteresis caused by diaphragm deformation does not sufficiently explain the results of an individual run. The hysteresis reported in manufacturer documentation was 1%. Further, if the hysteresis was a consequence of the sensor, it could be corrected by shifting the pressure values along the x-axis (excimer gas pressure). This translation does not explain the difference seen between the two parts of a trial results. Removing the

hysteresis also requires a shift along the y-axis (picoammeter current) in order to approach each other. Therefore there must be an additional aspect of the system which changes when pressure begins to decrease. A reasonable candidate for this difference between the charging and discharging sections of an individual trial is the minute amount of UV-absorbing gas which slowly desorbs into the gas plenum after the gas purges. It interferes with photon production and transport within the system until the vacuum is turned on and plenum pressure decreases. Because these UV absorbers are considerably lighter than the excimer gas in use, they are preferentially removed. As pressure is incrementally decreased further and UV absorbers are more removed, fewer photons are absorbed and the current increases.

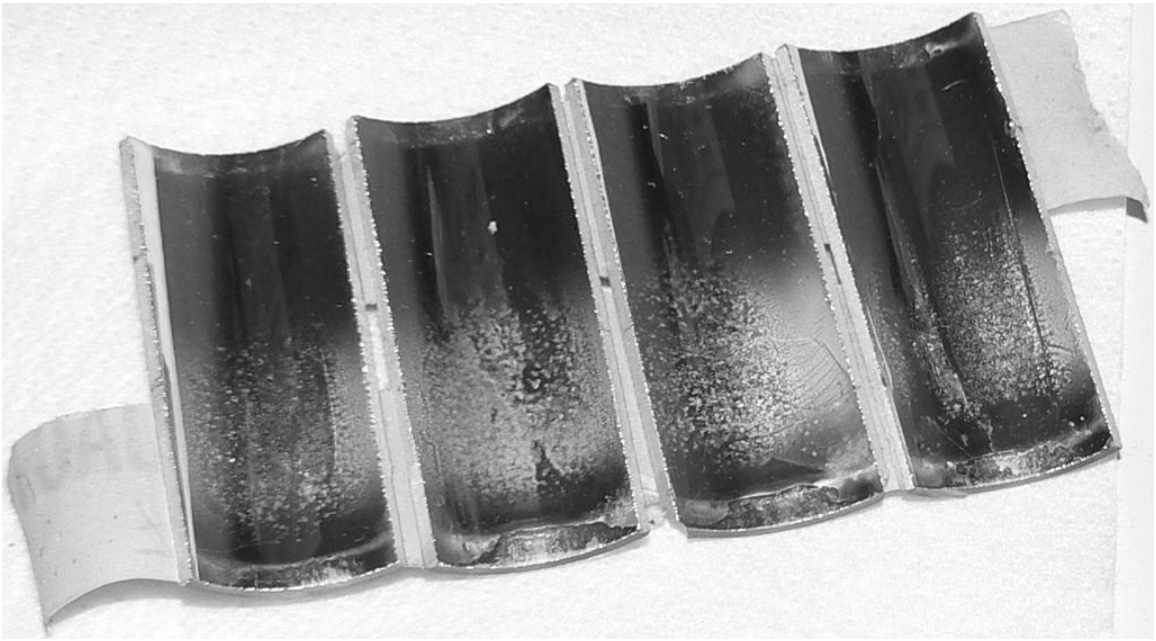

Figure 12: Radiation Damage to 51 mm Waveguide

Each trial consists of: an increase in photovoltaic current with pressure, a peak where pressure increase produces little change in photovoltaic current, and a decrease in photovoltaic current at pressures beyond the peak region. The light increase is expected,

as pressure increases, more energy is deposited in the gas and thus more light is produced, but the peak and decrease require some explanation. This observed photocurrent decrease is the result of mirror damage seen in Figure 12. Since increasing pressure causes a decrease α-particle range, the volume of gas which experiences ionization shrinks. This ionization region is also the photon-producing region, so the edge of the hemisphere which isotropically emits light also recedes from the photovoltaic as pressure increases. This increasing distance results in a decrease in the average solid angle of photon emission that overlaps the field of view of the photovoltaic cell. As a consequence, more photons must reach the photovoltaic by reflection off of the waveguide instead of reaching the photovoltaic by line of sight travel.

If the waveguide were reflecting properly, this would not be an issue. However the obvious waveguide damage in Figure 12 makes it clear that this is not the case. Instead of reflecting, photons which interact with the waveguide are absorbed. Thus more photons fail to reach the photovoltaic as pressure increases beyond the peak and the photocurrent decreases.

Table 7: Peak Results of Gas Fluorescer System

Experiment	Gas (Trial)	Activity (MBq)	I_{PV} (A)	R (A/W)	P_{PV} (W)	*Psrc* (W)
1	Ar-1	19.4	1.32E-10	0.165	8.00E-10	6.54E-06
	Ar-2	19.2	1.15E-10	0.165	7.09E-10	6.47E-06
	Ar-3	18.1	1E-10	0.165	6.06E-10	6.44E-06
	Xe-1	17.5	4.6E-11	0.114	4.04E-10	5.89E-06
	Xe-2	16.1	4.6E-11	0.114	3.80E-10	5.43E-06
2	Ar-4	9.8	2.82E-11	0.165	1.71E-10	7.84E-06
	Xe-3	7.8	7.90E-12	0.114	6.93E-11	2.67E-06

Table 8: Peak System Efficiencies of Gas Fluorescer System

Experiment	Gas (Trial)	ηtot (%)	ηd (%)	ηf (%)	ηtr (%)	ηPV (%)
1	Ar-1	5.16E-03	12.7	50	2.39	5.7
	Ar-2	4.62E-03	14.9	50	1.89	5.7
	Ar-3	4.19E-03	14.9	50	1.74	5.7
	Xe-1	2.89E-03	19.7	48	0.97	7.6
	Xe-2	2.95E-03	15.7	48	0.75	7.6
2	Ar-4	2.18E-03	25.5	50	2.25E-01	7.6
	Xe-3	2.59E-03	43.9	48	1.62E-01	7.6

The results of the two long-term trials of experiment 2 are found in Figure 13.The Argon trial exhibited stability because no additional mirror damage could accrue. Upon replacement of the 50 mm tube with the 75 mm tube before the Xenon trial, waveguide damage occurred once again. The lower source activity, higher average pressure, and higher LET of α-particles in Xenon resulted in an average damage which was lower than the rate of decrease between trials seen in experiment 1. The measured current decreased by thirty percent over 5 days. Although this decrease is undesired, this relative decrease in performance is less than that encountered by many alphavoltaics available in the literature. The photon transport efficiency for each trial was calculated using the photovoltaic current at the end of the experiment.

A plausible explanation for the shape of the current decrease shown in Figure 14 can be reasoned in a way analogous to radioactive decay. Consider a reflective surface that has been initially divided into N_0 individual regions. Any region can be rendered nonreflective if it incurs damage via α-particle interactions. This damage occurs at some rate λ, which is related to the source activity, and the rate of reflectivity loss for the

overall surface at any time is proportional to the number of regions *N* which remain reflective. So, the rate of damage for this system can be described as

$$\frac{dN}{dt} \sim -\lambda \cdot N$$

The solution to this equation is an exponential decrease over time. Mirror damage can be prevented by assembling, operating, and storing the system in an atmosphere with enough pressure to prevent α-particles from reaching the mirror surface.

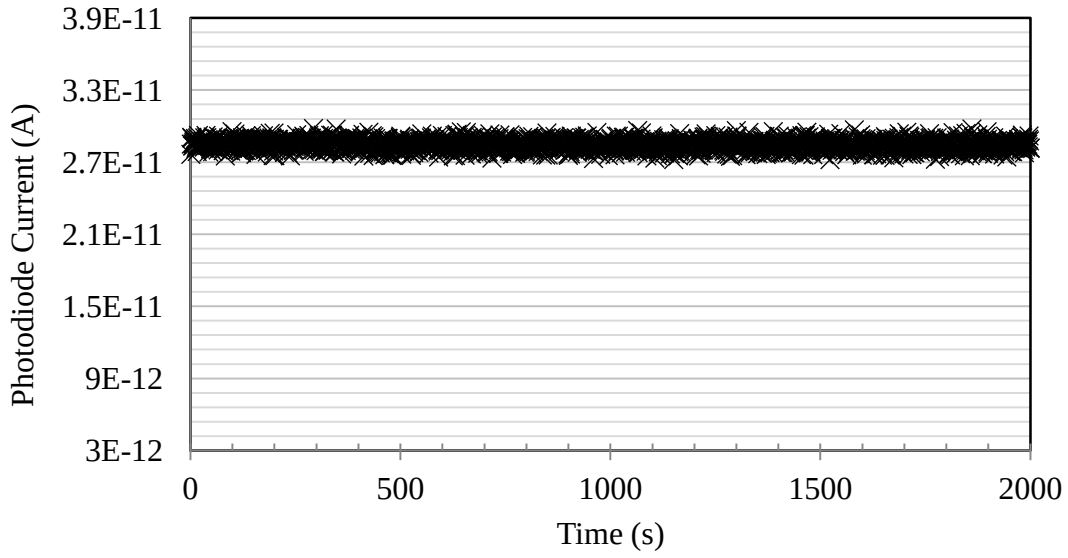

Figure 13: Photocurrent Stability Results, 30 Minute using Argon at 167 kPa

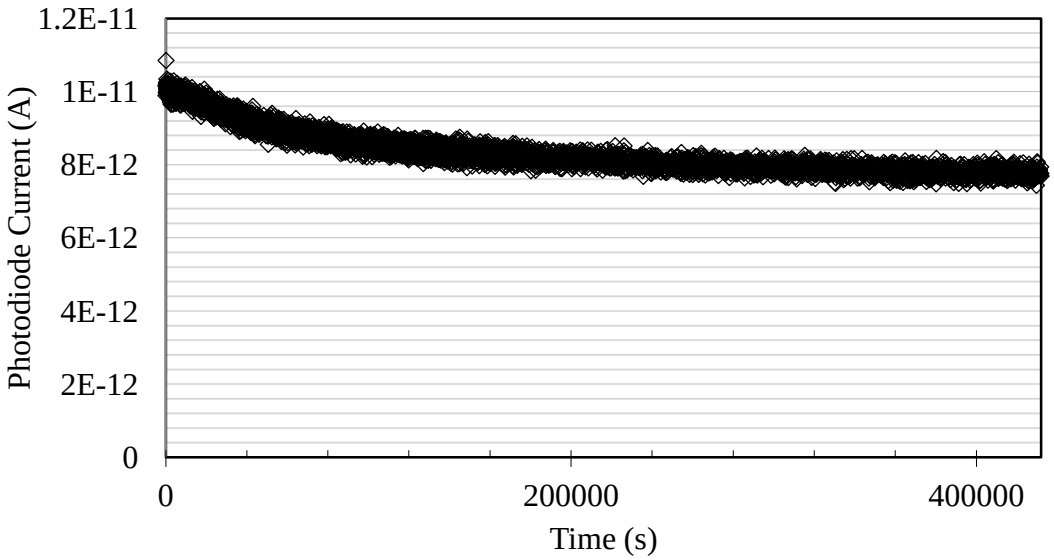

Figure 14: Photocurrent Stability Results, 5 Days using Xenon at 200 kPa

The mirror damage analogy was initially not a rigorous enough explanation. When other experiments using the Keithley picoammeter reported a similar exponential decrease in current, it was suspected that the decrease was a consequence of the device. If this were the case, determination and measurement of the actual current could not be achieved. To investigate this possibility the PMT was used in the long-term GaP fluorescer experiments as well, and the results were compared to the Keithley.

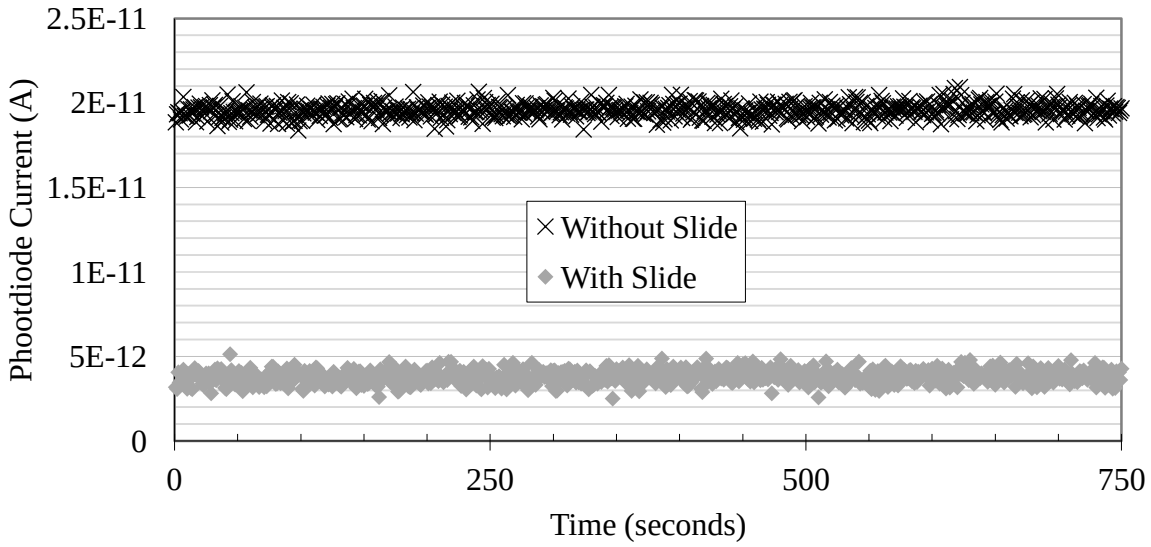

Figure 15: Filter Results for Ar, Gas Pressure 187 kPa

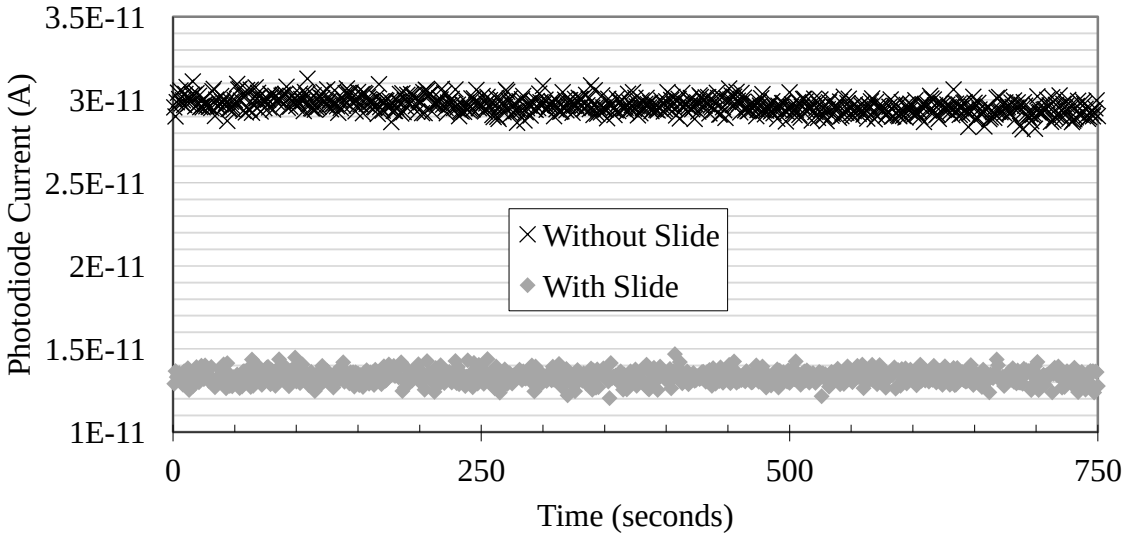

Figure 16: Filter Results for Xe, Gas Pressure 187 kPa

The results of the ultraviolet filter experiments in Figure 15 and Figure 16 reveal a significant photocurrent decrease upon introduction of the soda lime glass filter, a decrease of 80% for Argon and 55% for Xenon; after subtracting the 3.05×10^{-12} Amp

average dark current these percentages become 97% and 62%, respectively. This suggests that the systems are consistent with existing model results [26]: namely that a majority of interactions forms excimers which emit ultraviolet light upon decay.

6.2 Gallium Phosphide (GaP) Fluorescer

Table 9: GaP Performance Results Using Low-Activity Source

Trial	Position	Voltage	Current (nA)
0	0	-500	-0.192
	0	-600	-0.138
	0	-700	0.032
	0	-750	0.175
1	1	-750	0.150
	2	-750	0.255
2	0	-750	0.145
	1	-750	0.150
	2	-750	0.260
3	0	-750	0.145
	1	-750	0.135
	2	-750	0.255
	3	-750	0.140
	0	-750	0.140
	2	-750	0.250

The results for the GaP illumination experiment using the low-activity source are available in Table 9 and Figure 17. Detector current increases when α-particles illuminate the semiconductor crystal in position 2, which suggests that photons are being produced by the crystal as a result of ionization and radiative transition. The detector current decrease to dark current levels upon inclusion of the 550 nm line filter in position 3 suggests that the photons produced by the crystal are not those of the characteristic <100> phonon-assisted radiative transition. Spectrophotometry was unable to distinguish

any of the dominant radiative transitions from the background noise of the system. These results were confirmed using the OSI photovoltaic as shown in

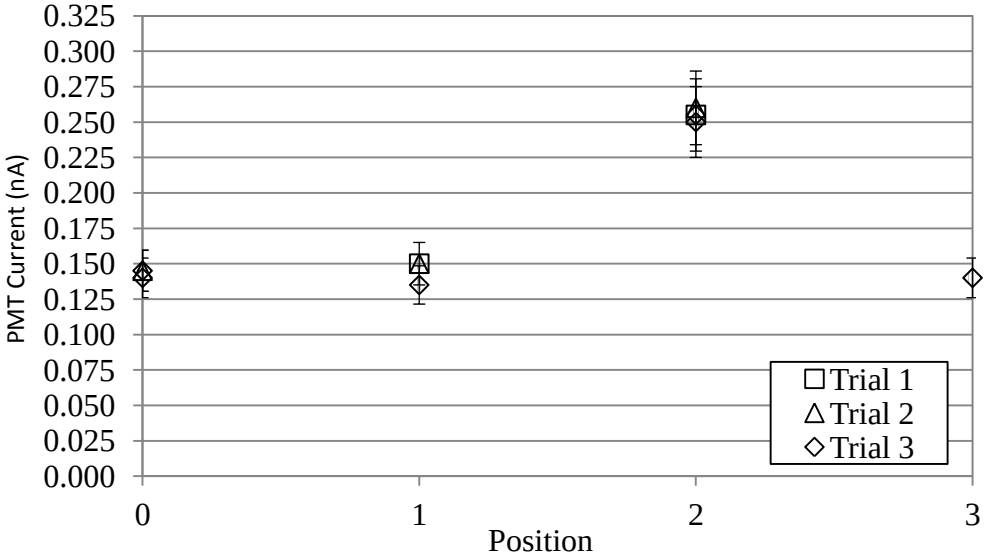

Figure 17: PMT Detector Current during GaP–α-Particle Interaction

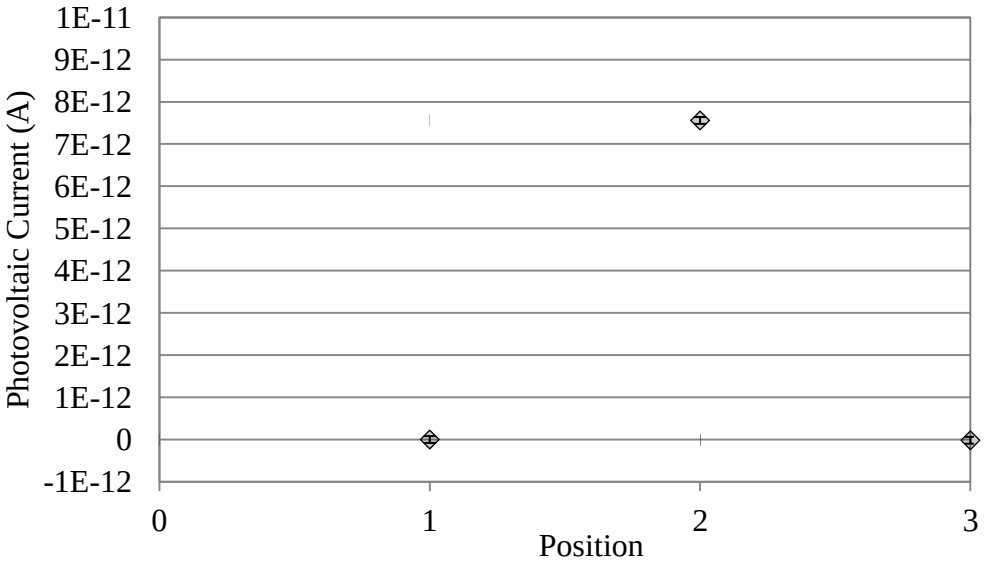

Figure 18: Photovoltaic Detector Current during GaP–α-Particle Interaction

The second experiment used the high-activity source; results are available in Figure 17 and Figure 18. The decay exhibited yields two results. First, the decay is

consistent between PMT and photovoltaic results. This indicates that both measurement systems either exhibit a common failure mode, or the decay observed during the gas fluorescer experiments was not due to malfunction of the Keithley. If both devices fail in a common way, then all results reported in this work are inaccurate. Second, the rate of defect introduction has a disproportionately large effect on light production. The traps produced by interactions serve as sites for electron capture and phonon scattering, which interferes with the process of direct and phonon-assisted radiative transitions. This decay makes GaP unsuitable as a fluorescer for long-lived nuclear batteries.

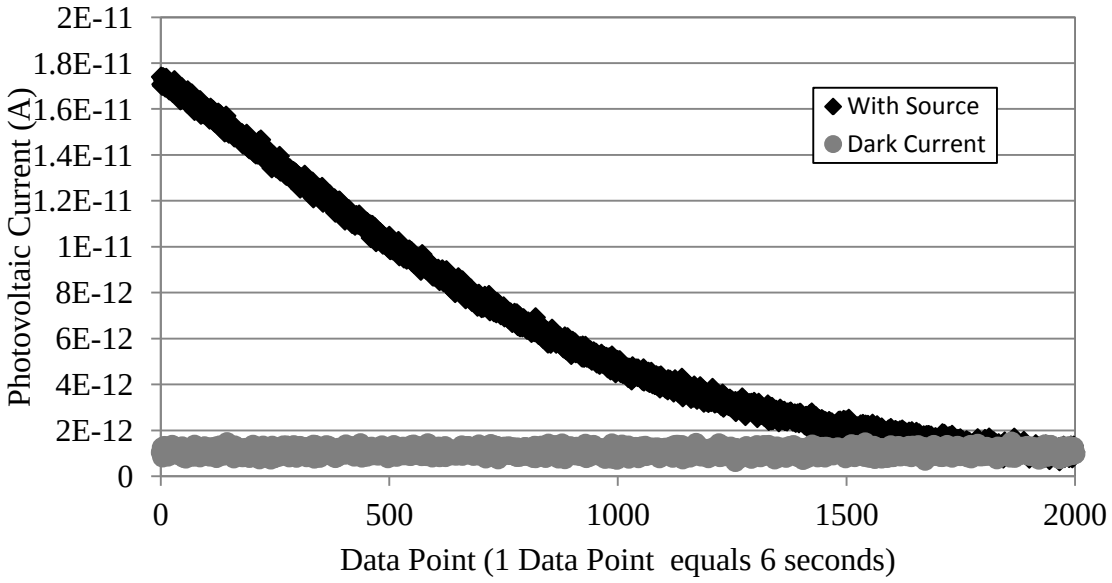

Figures 19: GaP Time-Dependent Performance Measured Using Photovoltaic Detector with High-Activity Source

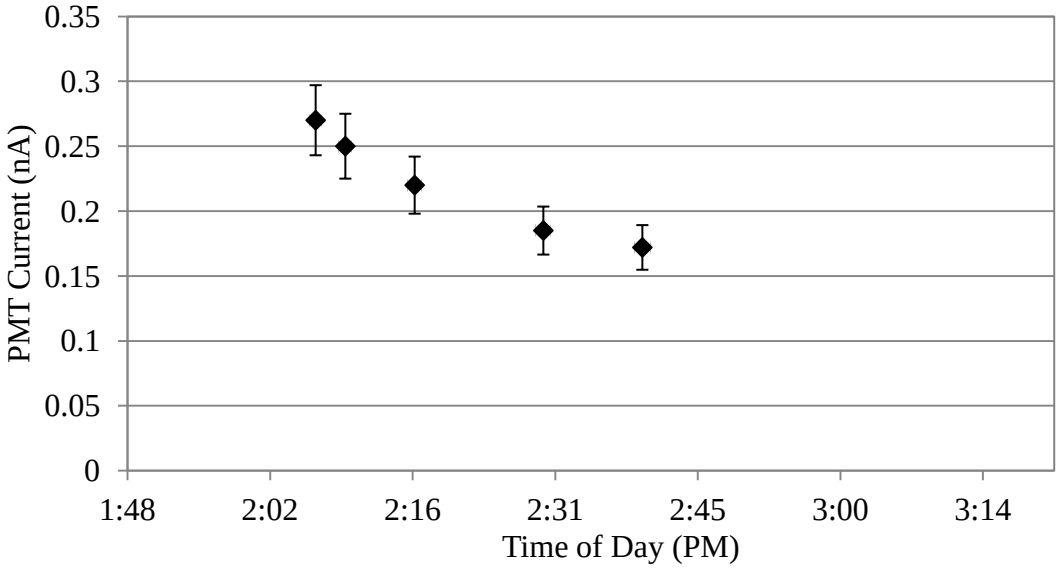

Figure 20: GaP Time-Dependent Performance Measured Using PMT Detector with High-Activity Source

7 CONCLUSIONS AND FUTURE WORK

Results of the two experimental systems were mixed. The gas fluorescer system did convert the energy α-particles emitted by Po-210 into electrical power via the photovoltaic with peak total conversion efficiency $(5.16 \pm 0.36) \times 10^{-3}$% and photon transport efficiency 2.4 ± 0.216%, too low to for use as a nuclear battery. Low total conversion efficiency is the result of 3 aspects of the system. Radiation damage to the waveguides incurred during low-pressure experiments and gas purging resulted in low transport efficiency. This radiation damage is avoided when the system is assembled, operated and stored in an environment of sufficient pressure to ensure that alpha particles are never able to reach the mirror; this can be accomplished by using a glove box capable of containing several atmospheres. Improvement of other system components which contributed to low total conversion efficiency is not so simple. Energy deposition efficiency can be doubled by minimizing the capsule which surrounds it, but this introduced hazards for safe handling. Currently fluorescer and photovoltaic conversion efficiencies are coupled in some sense. A different fluorescer can be used which has an energy closer to the bandgap of the photovoltaic, but fluorescers which emit in the visible part of the spectrum have lower fluorescer efficiencies than those which emit in the UV [21]. Higher band-gap photovoltaics allow higher photovoltaic conversion efficiencies with the use of UV emitters. Any of the other radioisotopes discussed in Ch. II could be used, but these would require additional precautions to protect the rest of the system from high-energy photon and neutron damage. These include isolation of the transport mechanism from the photon emissions common in other radioisotopes.

Ionization of the GaP crystal used in the solid-state fluorescer system during α-particle illumination triggered an increase in detector current. This suggests that the crystal initially produced some light, but the wavelength of this light could not be differentiated from the background. Further, α-particle flux emitted by the high-activity source damaged the capacity of the semiconductor to engage in radiative transition until detector current was indiscernible from the background. Solid-state systems appear to be poor candidates for long-lived systems, but research in PIDEC systems is ongoing within NSEI which uses other radiation-hard and direct band gap solid-state fluorescers.

BIBLIOGRAPHY

1. Engler, R., *Atomic Power in Space: A History*, U.S.DOE, Editor. 1987, DOE: Washington, DC. p. 188.
2. U.S.DOE. *Missions*. Space and Defense Power Systems [cited 2012 July 7]; Available from: http://www.ne.doe.gov/space/neSpace2c.html.
3. Anderson, D.J., *NASA Radioisotope Power Conversion Technology NRA Overview*, N.A.a.S. Administration, Editor. 2005, Glenn Research Center: Cleveland, OH. p. 15.
4. Bechtel, D., *Space Radioisotope Power Systems Advanced Stirling Radioisotope Generator*, U.S.DOE, Editor. 2011.
5. Miley, G.H., *Direct Conversion of Nuclear Radiation Energy*. Monograph Series on Nuclear Science and Technology, ed. J. Graham. Vol. I. 1970: American Nuclear Society. 518.
6. Hassan, M.H. and W.F. Faris. *Modeling of a Self Reciprocating Cantilever for a MEMS Nuclear Battery Powered by an Alpha Source*. in *Proceedings of the 2007 IEEE International Conference on Mechatronics and Automation*. 2007. Harbin, China: IEEE.
7. Li, H. and A. Lal, *Self-reciprocating radioisotope-powered cantilever.* Journal of Applied Physics, 2002. **92**(2): p. 6.
8. Duggirala, R., H. Li, and A. Lal, *High Efficiency β radioisotope energy conversion using reciprocating electromechanical converters with integrated betavoltaics.* Applied Physics Letters, 2008. **92**(15): p. 4.
9. Rybicki, G., C. Vargas-Aburto, and R. Uribe. *Silicon carbide alphavoltaic battery*. in *Conference Record of the Twenty Fifth IEEE Photovoltaic Specialists Conference, 1996.,*. 1996.
10. Qiao, D.-Y., et al., *A Micro Nuclear Battery Based on SiC Schottky Barrier Diode.* Journal of Microelectromechanical Systems, 2011. **20**(3): p. 685-690.
11. Fleurial, J.P., et al. *Solid-state power generation and cooling micro/nanodevices for distributed system architectures*. in *Thermoelectrics, 2001. Proceedings ICT 2001. XX International Conference on*. 2001.
12. Oh, K., et al., *The Theoretical Maximum Efficiency for a Linearly Graded Alphavoltaic Nuclear Battery.* Nuclear Technology, 2011.
13. Bailey, S.G., et al. *Photovoltaic development for alpha voltaic batteries*. in *Photovoltaic Specialists Conference, 2005. Conference Record of the Thirty-first IEEE*. 2005.
14. Cress, C.D., B.J. Landi, and R.P. Raffaelle, *InGaP alpha voltaic batteries: Synthesis, modeling, and radiation tolerance.* Journal of Applied Physics, 2006. **100**(11): p. 114519-114524.
15. Sychov, M., et al., *Alpha Indirect Conversion Radioisotope Power Source.* Applied Radiation and Isotopes, 2008. **66**(1): p. 173-177.
16. Cress, C.D., et al., *Alpha-particle-induced luminescence of rare-earth-doped Y2O3 nanophosphors.* Journal of Solid State Chemistry, 2008. **181**(8): p. 2041-2045.
17. Smith, A.W. and J. Turkevich, *Effect of Neutron Bombardment on a Zinc Sulfide*

Phosphor. Physical Review, 1954. **94**(4): p. 9.
18. Snyder, G.J., J. Patel, and J.-P. Fleurial, *Extremely-efficient, miniaturized, long-lived alpha-voltaic power source using liquid Gallium*, U.S.P. Office, Editor. 2004, The USA as represented by the Administrator of NASA: United States. p. 5.
19. Parkins, W.E., *Nuclear Battery Including Photocell Means*, U.S.P. Office, Editor. 1969, North American Rockwell Corporation: USA. p. 4.
20. Prelas, M.A., et al., *Nuclear Driven Flashlamps.* Laser and Particle Beams, 1987. **6**(1): p. 25-62.
21. Prelas, M.A., et al., *A Two-Step Photon-Intermediate Technique for the Production of Electricity, Chemicals or Lasers in Nuclear Energy Conversion.* Progress in Nuclear Energy, 1990. **23**(3): p. 223-240.
22. Schott, R.J., et al., *Photon Intermediate Direct Energy Conversion Using a Sr-90 Beta Source.* Nuclear Technology, 2012.
23. Prelas, M.A., *E-mail*, C. Weaver, Editor. 2012.
24. NNDC. *NuDat 2.6*. 2012 [cited 2012 July 2]; Available from: http://www.nndc.bnl.gov/nudat2/.
25. Carbaugh, E.H., *New Stochastic Annual Limits on Intake for Selected Radionuclides*, U.S.DOE, Editor. 2009, National Technical Information Service: Oak Ridge, TN. p. 10.
26. Chung, A., *Coupling and transport properties of ions generated by nuclear reactions for direct energy conversion*, in *Nuclear Science & Engineering Institute*. 1984, University of Missouri - Columbia: Columbia, MO. p. 215.
27. Messing, I., D.C. Lorents, and D.J. Eckstrom, *Low-Power Photolytically Pumped Lasers*. 1987, Southwest Research Institute: Livermore, CA. p. 70.
28. Lorents, D.C., D.J. Eckstrom, and D.L. Huestis, *Excimer Formation and Decay Processes in Rare Gases*, D.o.t. Navy, Editor. 1973, National Technical Information Service: Springfield, VA. p. 66.
29. Kiik, M.J., P. Dub, and B.P. Stoicheff, *Spectroscopic study of rare-gas excimer formation in direct-current discharge with supersonic expansion.* Journal of Chemical Physics, 1994. **102**(6): p. 14.
30. Pelowitz, D.B., *MCNPX User's Manual*. LA-CP-07-1473. 2008: Los Alamos National Lab.
31. *Band Structure and Carrier Concentration of Gallium Phosphide (GaP)*. New Semiconductor Materials. Characteristics and Properties [Electronic archive] 2001 [cited 2012; Available from: http://www.ioffe.ru/SVA/NSM/Semicond/GaP/bandstr.html.
32. *Eckert & Ziegler Reference & Calibration Sources: Product Information*, E.Z.I. Products, Editor. 2010: Valencia, CA.

VITA

Charles Weaver was born through a series of bangs, beginning with The Big One many years ago. The most recent resulted in his appearance in St. Louis, MO in 1982. After some things happened, he received a B.Sc. in Physics from Truman State University. Then more things happened and he received a M.Sc. in Nuclear Engineering from the NSEI at the University of Missouri. He enjoyed the teachers and town so much that he stayed, and by now has received his Ph.D. Hopefully.